Pergamon

Journal of Structural Geology, Vol. 17, No. 10, pp. 1375 to 1385, 1995

0191-8141/95 $9.50 + 0.00

0191-8141(95)00032-1

Analysis of geologic strain data in strain-magnitude space

MARK T. BRANDON

Kline Geology Laboratory, Yale University, P.O. Box 208109, 210 Whitney Avenue, New Haven, CT 06520-8109, U.S.A.

(*Received* 13 *May* 1994; *accepted in revised form* 14 *March* 1995)

Abstract—Strain-magnitude space is defined by an orthogonal coordinate system using the natural principal strains E_x, E_y, E_z. Distance from the origin provides an invariant measure of total-strain magnitude E_t, which can be decomposed into two orthogonal components: volume E_v and deviatoric E_d strain. The volume-strain axis E_v is equidistant from the E_x, E_y, E_z axes, and the E_d component lies in an orthogonal section called the deviatoric section. E_v and E_d are independent of the rotational component of the deformation and are shown to be fundamental measures of strain magnitude.

The deviatoric section contains the Flinn and Nadai diagrams, which are commonly used to identify strain symmetry (oblate vs prolate). The Nadai diagram is preferred because it provides an undistorted representation of the deviatoric section. Other sections that include the volume-strain axis are better suited for distinguishing strain type (flattening vs constriction).

Strain-magnitude space ignores the directional information contained in strain-tensor data. This leads to a significant bias which is illustrated by comparing a strain-magnitude distribution with its average, as determined by a tensor-averaging method. The mode of the distribution will generally give an unbiased estimate of the average volume strain and an estimate of the average deviatoric strain on the high side.

INTRODUCTION

An important objective in structural geology is the quantitative measurement and analysis of deformation associated with the development of geologic structures, both large and small. A complete characterization of distortion, rotation, and dilation associated with a general deformation at a material point requires specification of the nine components of the deformation-gradient tensor. Most studies, however, focus only on the directions and relative magnitudes of the principal strains because these measurements are generally fairly easy to make (e.g. Ramsay & Huber 1983). In fact, the plots most commonly used to analyze strain data, such as the Flinn and Nadai diagrams (Flinn 1962, 1978, Nadai 1963, pp. 70–76, Hsu 1966, Hossack 1968), are designed specifically to display relative strain measurements. Ramsay & Wood (1973), Hobbs *et al.* (1976), and Ramsay & Huber (1983), among others, have given careful consideration to the limitations of these diagrams, especially for those cases involving significant volume strain. Nonetheless, these diagrams by themselves do not provide an adequate representation of the full variability of strain-magnitude data.

Nadai (1950, 1963), Hsu (1966), and Elliott (1972) introduced the idea of using the natural principal strains—equal to the logarithm of the principal stretches—to define a three-dimensional 'strain-magnitude' space (Fig. 1). Nadai (1963), Hsu (1966), and Hossack (1968) proposed displaying relative strain data on the octahedral plane of this strain-magnitude space (Figs. 1b & c). The resulting plot has been called a Hsu diagram (Hobbs *et al.* 1976, p. 37) but Nadai diagram seems more appropriate (Flinn 1978) given the precedence of Nadai's (1963, pp. 70–75) publication. Nadai (1963) also provided an early discussion of the concept of a strain path (cf. Flinn 1962, 1978, Elliott 1972), with a particular focus on the relationship between deformational work and the distance in strain-magnitude space. Flinn (1978, p. 294) and Ramsay & Huber (1983, pp. 202–203), among others, have discounted the Nadai diagram, because the relationship between work and distance is not applicable for non-coaxial deformations. This conclusion overlooks the broader physical significance of distance in strain-magnitude space, a point that is developed below.

My objective here is to review the concept of strain-magnitude space and to demonstrate its advantages for interpretation of both relative and absolute strain data. As an example dataset, I use the results of a strain study by Ring & Brandon (1994) of sandstones from the eastern part of the Franciscan Complex of California, which was accreted and deformed in an accretionary wedge under high pressure–low temperature conditions during the Cretaceous and Early Cenozoic (Yolla Bolly and Valentine Springs units: Blake *et al.* 1988, Jayko & Blake 1989). The strain measurements are based on dimensional changes of detrital grains which have been truncated by the development of a pressure-solution cleavage and on the modal abundance of directed fiber overgrowths (Brandon *et al.* 1994). The final results include estimates of the directions and absolute magnitudes of the principal stretches. These data are used here to illustrate general concepts. The strain measurement methods and geologic interpretations will be presented elsewhere.

STRAIN-MAGNITUDE SPACE

Six independent variables are required to fully specify the finite strain at a material point. The usual convention

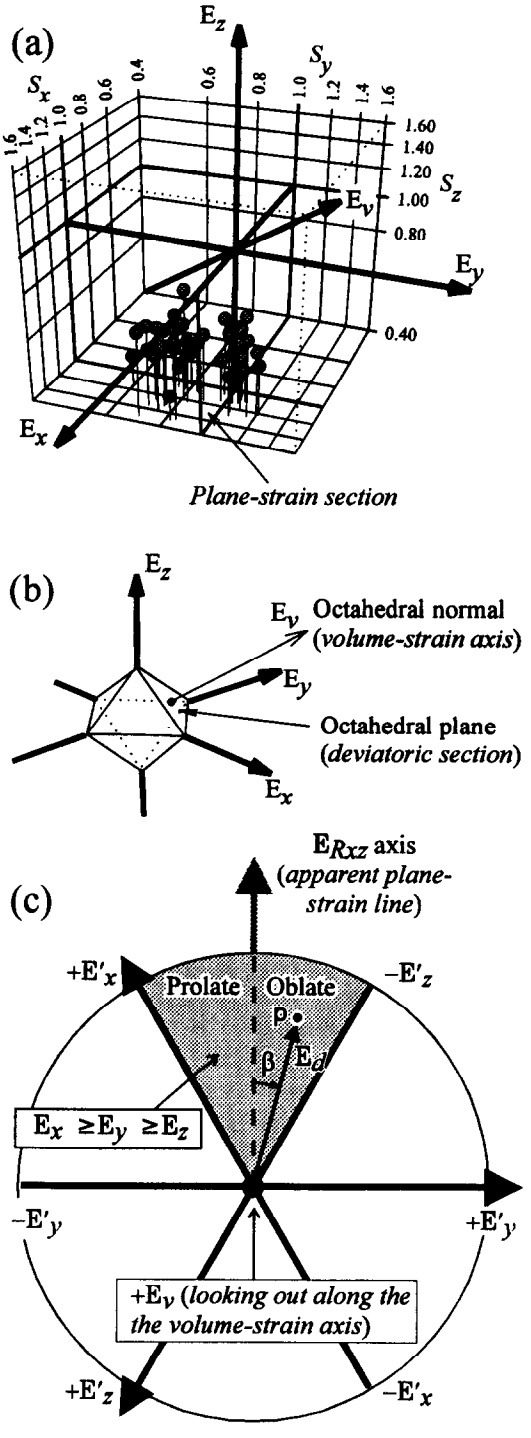

Fig. 1. (a) Three-dimensional plot of strain-magnitude space. Logarithmic axes ensure that the space is properly scaled for the natural principal strains E_x, E_y, E_z, while retaining the more familiar measure of stretch S_x, S_y, S_z as the units for the axis tick labels. The diagonal axis labeled E_v is the volume-strain axis. Strain data are for sandstones of the eastern Franciscan Complex, California (Ring & Brandon 1994). (b) Layout showing the geometry of the octahedral normal and octahedral plane, which correspond to the volume-strain axis and the deviatoric section, respectively. (c) The deviatoric section is formed by projecting data parallel to the volume-strain axis onto the octahedral plane. The shaded sector shows the area covered by the Flinn and Nadai diagrams. The boundaries of this sector are defined by the convention $E_x \geq E_y \geq E_z$. The axes show the projected form of the E_x, E_y, E_z axes as viewed looking down the volume-strain axis. They are rescaled as natural principal deviatoric strains E'_x, E'_y, E'_z, where deviatoric strain is defined as $E' = E - E_v/3$.

is to use three variables to describe the orientation of the principal strain directions (e.g. Euler angles) and the remaining three variables to describe the magnitude of the principal strains, as represented by the principal elongations, e_x, e_y, e_z, or the principal stretches, S_x, S_y, S_z. Elongation is defined as $e = (l_f - l_i)/l_f$, and stretch as $S = l_f/l_i$, where l_i and l_f are the initial and final lengths of a material line. The subscripts x, y, z refer to maximum extension, intermediate, and maximum contraction, where $e_x \geq e_y \geq e_z$ and $S_x \geq S_y \geq S_z$. The vectors **x**, **y**, **z** indicate the orientations of the principal strain axes.

The principal strains are invariants of the strain tensor because they remain unaffected by changes in the reference frame (i.e. invariant upon transformation). Other variables can be used as invariants. In fact, one of our objectives is to find a set of invariants that more clearly illustrates the magnitude information contained in a strain tensor (cf. Ramsay & Huber, 1983, p. 200).

The ideal plot for representing strain magnitudes would be a Euclidean vector space where orthogonal axes and distance are clearly defined. Neither the principal stretches nor the principal elongations are suited for this application. Stretch is an asymmetric measure, with contraction occupying a range 0 to 1, and extension, 1 to ∞. During deformation, each strain increment causes dimensional changes that are proportional to the current dimensions of the deforming material. As a result, both elongation and stretch accumulate nonlinearly (Nadai 1950, 1963). If these measures were used to construct a strain-magnitude space, the distance between points in the space would lack any clear physical significance because of the nonlinear relationship between the strain increments and the integrated result.

The natural principal strains, E_x, E_y, E_z, provide a useful basis for constructing a strain-magnitude space. Natural strain is defined by $E = \ln(S)$ and has the same units as elongation (ln indicates the natural logarithm). The upper-case epsilon E is preferred here to the more commonly-used symbols ε or $\bar{\varepsilon}$ because ε is sometimes used to represent elongation and because the overbar used for $\bar{\varepsilon}$ can be taken as indicating an average value. The concept of natural strain originated from the observation that the longitudinal stretch in a rod extended at a constant strain rate $\dot{e}$ accumulates logarithmically with time (cf. Nadai 1950, p. 131), as indicated by

$$E(\tau) = \ln S(\tau) = \ln\left(\frac{l_f}{l_i}\right) = \int_{l_i}^{l_f} \frac{dl}{l} = \int_{t=0}^{t=\tau} \dot{e}dt = \dot{e}\tau, \quad (1)$$

where l represents the length of the rod as a function of time, and τ indicates the total duration of the deformation. The reason that stretch accumulates nonlinearly is that for each strain increment, the change in length of a material line is relative to the current length of the line. Nadai (1937) introduced the term 'natural strain' to emphasize that E represents the strain relative to the evolving length of the material (i.e. the natural state), as opposed to the initial length, as is commonly the practice for experimental deformation. Ramsay & Huber (1983, p. 281) objected to this term and suggested 'logarithmic

strain' as an alternative, but this is unsatisfactory because some natural strain parameters are not related to the logarithm of their conventional counterparts (e.g. natural vs conventional octahedral shear strain; compare equations 10 and 12).

Following Nadai (1963) and Elliott (1972), the natural principal strains are used to define a Euclidean vector space with points in the space defined by the position vector $E_t\hat{\mathbf{r}} = E_x\hat{\mathbf{i}} + E_y\hat{\mathbf{j}} + E_z\hat{\mathbf{k}}$, where $\hat{\mathbf{r}}$ is a unit vector representing the orientation of the position vector and $\hat{\mathbf{i}}$, $\hat{\mathbf{j}}$, $\hat{\mathbf{k}}$ are an orthogonal set of unit vectors. Distance is defined in the usual fashion; for example,

$$E_t = \sqrt{E_x^2 + E_y^2 + E_z^2} \qquad (2)$$

gives the distance from the origin. In this regard, E_t can be viewed as an invariant measure of the total magnitude of the strain tensor. An example of this three-dimensional space is shown in Fig. 1(a). Note that the axes of the plot are scaled logarithmically and labeled using units of stretch. In this manner, we can introduce correctly scaled axes while retaining stretch as a more familiar measure of strain.

VOLUME-STRAIN AXIS

Another invariant for the strain tensor is volume strain, which is represented here as volume stretch, $S_v = V_f/V_i$, where V_i and V_f are the initial and final volumes of a 'representative elementary volume' (REV). The REV is defined by a set of material points that mark the boundary of a closed three-dimensional surface, usually taken to be a sphere of unit radius. Consideration of the transformation of a unit sphere into a deformed ellipsoid indicates the following simple relationship between the principal stretches and the volume stretch: $S_v = S_xS_yS_z$. Using natural strains, this relationship is $E_v = E_x + E_y + E_z$, where E_v is the natural volume strain.

In strain-magnitude space, we can identify a volume-strain axis oriented at equal angles to the E_x, E_y, E_z axes (E_v in Fig. 1). This direction is called the octahedral normal (or space diagonal) because it is normal to the octahedral plane (Fig. 1b). These terms refer to a hypothetical octahedron symmetrically oriented with respect to the origin and the E_x, E_y, E_z axes (Fig. 1b). For our purposes, the octahedral normal and octahedral plane contain a new set of axes that can be used to span strain-magnitude space. A volume strain would appear as a translation parallel to the octahedral normal, whereas a distortional strain would appear as a translation in some direction parallel to the octahedral plane.

Several factors can contribute to the overall volume stretch, as illustrated by the following equation (modified from Brimhall & Dietrich 1987):

$$S_v = \left(\frac{1-n_i}{1-n_f}\right)\left(\frac{\rho_i}{\rho_f}\right)\left(\frac{m_f}{m_i}\right) = S_nS_\rho S_m, \qquad (3)$$

where n is the average porosity as a fractional ratio, ρ is the average grain density, and m is the solid mass inside the REV. The subscripts i and f indicate the initial and final states. The terms in (3) can be represented as three volume-stretch components, S_n, S_ρ, and S_m, whose product equals S_v, the total volume stretch. S_n is the volume stretch due to a net change in pore fluid content inside the REV, with compaction of sediments representing a familiar example. S_ρ is the volume stretch produced by changes in the average mineral density within the REV, as might result from diagenetic or metamorphic reactions (i.e. polymorphic transformations, solid–solid reactions, devolatilization reactions, etc.). S_m is the volume stretch due to transport of the solid component of the rock over a length scale greater than that defined by the REV. This type of strain is called a *mass-transfer volume strain* and most commonly occurs by dissolution, transport, and precipitation in the presence of a moving fluid. Common examples include the formation of stylolites and veins.

From the view point of continuum mechanics, a volume stretch is defined as an isotropic change in volume at a point. An idea that comes up frequently in discussions is the possibility of introducing an anisotropic volume-change tensor to represent the directional aspects of the volume-change process. In principle, there is nothing wrong with this approach, but in practice, its application will be limited to certain simple types of deformation where at least one of the principal stretches remained unchanged and where the mechanisms responsible for the volume change operated coaxially with those responsible for any closed-system distortion. Examples might include basinal compaction of sediment or plane-strain pressure solution. As a counter example, consider the case of a constrictional deformation involving contraction by dissolution in the **y** and **z** directions, extension in the **x** direction by the formation of fiber overgrowths, and a volume strain by mass loss as indicated by $E_x + E_y + E_z$. For this case, there is no way to separate the relative contributions that dissolution in the **y** and **z** directions have made to the overall mass loss. As a result, we do not have enough information to resolve an anisotropic volume-change tensor. Thus, it is my conclusion that the conventional isotropic measures, such as S_v and E_v, provide a more widely applicable representation of the volume-change process.

DEVIATORIC STRAIN

The distortional aspect of the strain can be represented by projecting strain-magnitude data onto the octahedral plane to form what is called here the *deviatoric section*. In this section, the E_x, E_y, E_z axes are now represented by the principal deviatoric strains, either E'_x, E'_y, E'_z or S'_x, S'_y, S'_z. The natural deviatoric strains are defined by the relationship: $E' = E - E_v/3$, and the deviatoric stretches by: $S' = S/S_v^{1/3}$. These measures can be viewed as relative strains normalized to a constant volume, so that $E'_x + E'_y + E'_z = 0$ and $S'_x S'_y S'_z = 1$.

The more familiar measures of deviatoric strain are the principal axial ratios, R_{xy}, R_{yz} and R_{xz}, which have the following relationships:

$$\begin{aligned} E_{Rxy} &= \ln R_{xy} = \ln(S_x/S_y) = E_x - E_y = E'_x - E'_y, \\ E_{Ryz} &= \ln R_{yz} = \ln(S_y/S_z) = E_y - E_z = E'_y - E'_z, \\ E_{Rxz} &= \ln R_{xz} = \ln(S_x/S_z) = E_x - E_z = E'_x - E'_z. \end{aligned} \quad (4)$$

E_{Rxy}, E_{Ryz}, E_{Rxz} are used as a short-hand notation for the logarithm of the principal axial ratios. Nadai (1937, his equation 21) called these the natural principal shears.

Because of the convention $E_x \geq E_y \geq E_z$, the only accessible part of the deviatoric section is the sector bounded by the $+E'_x$ and $-E'_z$ axes (Fig. 1c). This sector marks the region covered by both the Flinn and Nadai diagrams (Fig. 2). The only difference between these diagrams is that $+E'_x$ and $-E'_z$ axes are rotated into an orthogonal orientation in the Flinn diagram (Fig. 2a). Thus, the Flinn diagram is somewhat easier to construct but the Nadai diagram (Fig. 2b) retains an undistorted representation of the deviatoric section. The E_{Rxz} axis (Fig. 1c) coincides with the *apparent plane strain line* because the points that plot on this line indicate a plane-strain deformation ($S_y = 1$, $E_y = 0$) but only if the deformation is isochoric (i.e. constant volume: $S_v = 1$, $E_v = 0$). This relationship is illustrated by the geometry of the axes in the deviatoric section (Fig. 1c): the E_{Rxz} axis is perpendicular to the E'_y axis and intersects that axis at $E'_y = 0$.

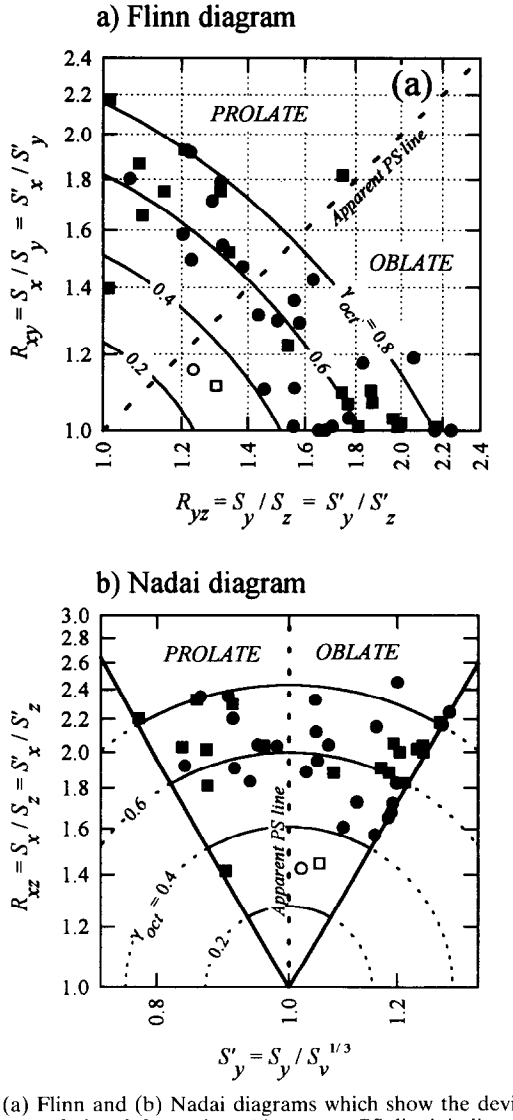

Fig. 2. (a) Flinn and (b) Nadai diagrams which show the deviatoric component of the deformation. 'Apparent PS line' indicates the apparent plane-strain line. Strain data are for sandstones of the eastern Franciscan Complex as exposed in the Yolla Bolly Mountains (squares) and the Diablo Range (circles) (Ring & Brandon 1994). The open symbols indicate tensor averages as determined by the method in Appendix A. Contours show the magnitude of conventional octahedral shear γ_{oct}, which is a measure of the average distortion. See Appendix B for details about the construction of the Nadai diagram.

The Flinn and the Nadai diagrams are useful for distinguishing the relative shapes of the strain ellipsoids, whether prolate (cigar-shaped) or oblate (pancake-shaped). Following Hossack (1968), this classification is called *strain symmetry*. If one can make the assumption that the deformation was isochoric, then strain symmetry can be used to infer *strain type* (Ramsay & Huber 1983, p. 171), whether constrictional ($S_y < 1$, $E_y < 0$), plane strain ($S_y = 1$, $E_y = 0$), or flattening ($S_y > 1$, $E_y > 0$). In my opinion, the interpretation of strain type using strain symmetry alone is not warranted because assumptions about volume strain are difficult to justify in the absence of data.

PHYSICAL SIGNIFICANCE OF DISTANCE IN STRAIN-MAGNITUDE SPACE

We have seen that the natural principal strains E_x, E_y, E_z, which are invariants of the strain tensor, can be used to define a space where distance is proportional to strain magnitude. If we erect an alternative coordinate system to span this space, the new variables would represent another set of invariants. The cylindrical coordinates E_v, E_d, and β are conceptually useful because the total strain magnitude is decomposed into two more familiar orthogonal components: volume strain E_v, and deviatoric strain E_d, as indicated by:

$$E_t = \sqrt{E_d^2 + E_v^2}. \quad (5)$$

Natural deviatoric strain E_d is more commonly represented by the symbols ε_s and $\bar{\varepsilon}_s$ (Nadai 1963, Ramsay & Huber 1983); the subscript d is used here to make it clear that E_d refers to the deviatoric strain and not the total strain. E_d is defined as the projected distance of $E_t\hat{\mathbf{r}}$ in the deviatoric section, which is given by (Nadai 1963, pp. 50 and 73):

$$\begin{aligned} E_d &= \sqrt{1/3}\sqrt{(E_x - E_y)^2 + (E_y - E_z)^2 + (E_x - E_z)^2} \\ &= \sqrt{E'^2_x + E'^2_y + E'^2_z}. \end{aligned} \quad (6)$$

This equation describes a cylinder of radius r centered on the volume-strain axis, as indicated by the following general equation:

$$r^2 = (x - y)^2 + (y - z)^2 + (x - z)^2. \quad (7)$$

In the deviatoric section, these cylinders would appear as a nested set of circles centered on the origin. The

variable β indicates the clockwise orientation of E_d in the deviatoric section with respect to the E_{Rxz} axis (Fig. 1c). This variable can be viewed as an angular version of the Lode's parameter ν (e.g. Hossack 1968), where: $\nu = \sqrt{3} \tan \beta$.

For purposes of plotting, it is useful to specify the cylindrical coordinates E_v, E_d, and β in terms of an orthogonal set of variables: E_{Rxz}, E'_y, E_v (Fig. 1c). Substitution of these variables into (5) and (6) gives:

$$E_t\hat{\mathbf{r}} = \sqrt{1/2}\, E_{Rxz}\hat{\mathbf{I}} + \sqrt{3/2}\, E'_y \hat{\mathbf{m}} + E_v \hat{\mathbf{n}} \qquad (8)$$

and

$$E_d = \sqrt{(1/2)\, E^2_{Rxz} + (3/2)\, E'^2_y}, \qquad (9)$$

where $\hat{\mathbf{I}}$, $\hat{\mathbf{m}}$, $\hat{\mathbf{n}}$ are basis vectors for the E_{Rxz}, E'_y, E_v coordinate system.

Nadai (1963, pp. 43–105) made the interesting observation that under certain circumstances, strain magnitude could be related to deformational work. In this context, deformational work is the work associated with internal deformation of a material and should not be confused with the total work done on the system (Malvern 1969, p. 227). Nadai (1963) focused on E_d as an indirect measure of the *distortional work* because his interest was in the deformation of metals where volume strains are negligible. For geologic deformation, we need to include the *dilational work* associated with producing a volume strain (Nadai 1963, p. 43). Inspection indicates that Nadai's (1963) analysis is applicable for this more generalized case, but the conclusions we might draw are still fairly restrictive.

(1) For coaxial deformation of isotropic linear ductile materials (e.g. perfect plasticity, linear viscosity, etc.), the length of the strain path is proportional to the deformational work (Nadai 1963, p. 87).

(2) For isotropic ductile materials, including those with nonlinear constitutive properties (e.g. strain-hardening plasticity, power-law viscosity, etc.), a coaxial deformation with a straight strain path requires the least amount of deformational work to achieve a specified strain magnitude. Possible exceptions to this conclusion might arise for materials that have constitutive properties that are dependent on the deformation path.

The conceptual link between work and strain magnitude is useful, but the conclusions above show that this idea has only limited application. A more useful physical interpretation is to view strain magnitude as a measure of deformation, and not of work. In this context, E_v and E_d represent fundamental measures of volumetric strain and deviatoric strain. The interpretation of E_v is already clearly defined, but what about E_d?

The physical interpretation of E_d can be illustrated by reference to two measures of octahedral shear strain. The first is Γ_{oct}, the natural octahedral shear strain, which is proportional to E_d according to the relationship: $E_d = \sqrt{3/4}\, \Gamma_{oct}$. Natural octahedral shear strain is typically represented by $\bar{\gamma}_{oct}$, but an upper-case Γ_{oct} is used here to avoid the bar overstrike and to be consistent with the upper-case epsilon used for natural strain. To describe Γ_{oct}, we want to view the octahedral plane and octahedral normal as spatial features defined at each point within the deforming material by the orientation of the principal axes of the evolving finite strain tensor for that point. Nadai (1963, p. 73) defined Γ_{oct} as the time integral of the instantaneous shear strain rate acting on the octahedral plane. Note that Γ_{oct} is not related to any material line, but instead represents the integrated angular distortion experienced by those material lines and planes that pass through the octahedral normal and octahedral plane, respectively (Nadai 1950, pp. 115 and 132). Because orientation is defined with respect to the principal finite strain directions, Γ_{oct} is solely a function of the principal deviatoric strains and is entirely independent of the rotational component of the deformation. This conclusion is demonstrated by the full equation for the natural octahedral shear strain:

$$\begin{aligned}\Gamma_{oct} &= 2/3\, \sqrt{(E'_x - E'_y)^2 + (E'_y - E'_z)^2 + (E'_x - E'_z)^2} \\ &= \sqrt{(2/3)\, E^2_{Rxz} + 2\, E'^2_y}. \end{aligned} \qquad (10)$$

Contour surfaces of Γ_{oct} have the same form as those for E_d (cf. 6, 9). In particular, contours of Γ_{oct} appear in the Nadai diagram as a series of nested circles centered on the origin.

As a fundamental measure of deviatoric strain magnitude, Γ_{oct} is flawed because it does not track the distortion of any specific material features. A useful alternative is the conventional octahedral shear strain γ_{oct} which is defined as the amount of shear strain recorded by a material line and material plane that start with orientations parallel to the octahedral normal and octahedral plane, respectively. To determine the final orientations of these features, we would need to know both the strain and the rotation for the deformation. If instead, we are only interested in the magnitude of the octahedral shear strain γ_{oct}, then the principal deviatoric strains are sufficient.

To demonstrate this point, consider the general equation for finite shear strain γ (Jaeger & Cook 1979, p. 457) as a function of the initial orientation of a material line defined by the direction cosines l, m, n. The coordinate frame is defined by the initial directions of the principal finite strains in the unstrained state:

$$\begin{aligned}\gamma^2 = {} & [S'_x(S'^2_y - S'^2_z)mn]^2 + [S'_y(S'^2_x - S'^2_z)nl]^2 \\ & + [S'_z(S'^2_x - S'^2_y)lm]^2. \end{aligned} \qquad (11)$$

Substitution of the direction cosines $\sqrt{1/3}$, $\sqrt{1/3}$, $\sqrt{1/3}$ for the octahedral normal into (11) and simplification gives:

$$\gamma_{oct} = 2/3\, \sqrt{\sinh^2(E'_x - E'_y) + \sinh^2(E'_y - E'_z) + \sinh^2(E'_x - E'_z)} \qquad (12)$$

and

$$\gamma_{oct} = 2/3\, \sqrt{\cosh^2(E_{Rxz}) + \cosh(E_{Rxz}) \cosh(3E'_y) - 2}, \qquad (13)$$

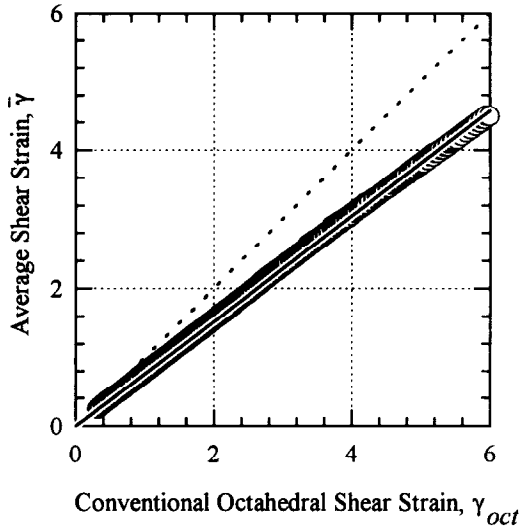

Fig. 3. Comparison of the conventional octahedral shear strain γ_{oct} with the average shear strain $\bar{\gamma}$. γ_{oct} was calculated using equation (13) and $\bar{\gamma}$ was determined by numerical integration of (11). Data values (open circles) were calculated for a range of geologically representative strain values (R_{xy} = 1.0 to 6.0, and S'_y = 0.25 to 4.0). The data are well fitted by the relationship: $\bar{\gamma} \approx 0.761\ \gamma_{oct}$, which has average residuals of ~1.1 percent relative to expected values for $\bar{\gamma}$.

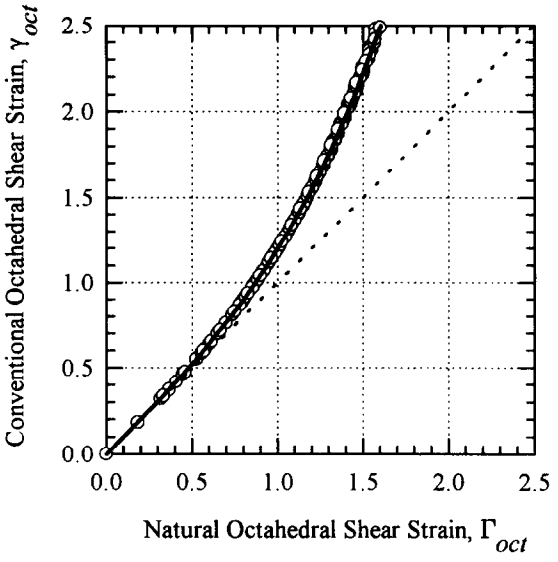

Fig. 4. Comparison of natural octahedral shear strain Γ_{oct} with conventional octahedral shear strain γ_{oct}. The solid line indicates the approximate relationship between γ_{oct} and Γ_{oct} as given by (14). Exact values are indicated by the open symbols and were determined by (10, 12) for the range R_{xz} = 1.0 to 6.0, and S'_y = 0.25 to 4.0.

where the hyperbolic sine and cosine are defined as $\sinh(x) = (e^x - e^{-x})/2$ and $\cosh(x) = (e^x + e^{-x})/2$.

To illustrate the physical significance of γ_{oct}, consider the following example. Conventional shear strain γ is related to angular shear strain ψ by: $\gamma = \tan \psi$. Thus, if $\gamma_{oct} = 1$, the final angle between the material line and material plane that originated at the octahedral normal and octahedral plane, respectively, would be arctan (1) = 45°. The octahedral shear strain can be viewed as a measure of the average distortion produced by the strain tensor because the starting position, the octahedral normal, has an orientation equidistant from all three principal strain directions. In this context, it is worth comparing γ_{oct} to the average shear strain $\bar{\gamma}$ at a point, which can be calculated by numerical Monte Carlo integration of (11) with respect to l, m, n using an initially random distribution of material lines (Press *et al.* 1992, p. 155). The results of this calculation are shown in Fig. 3, as determined for a range of geologically representative strain values (R_{xy} = 1.0 to 6.0, and S'_y = 0.25 to 4.0). The data show that the octahedral shear strain is proportional to the average shear strain, as indicated by the following approximate relationship: $\bar{\gamma} \approx 0.761\ \gamma_{oct}$. This exercise demonstrates that γ_{oct} is, in fact, a fundamental measure of the average distortion, and is independent of the rotational and volumetric components of the deformation. Note that $\bar{\gamma}$ is probably preferred over γ_{oct} because it provides a direct measure of the average shear strain, but any advantages are outweighed by the greater effort needed to calculate $\bar{\gamma}$.

To my knowledge, there is no closed-form analytical expression that relates γ_{oct} to Γ_{oct}. Numerical calculations indicate that γ_{oct} is not solely dependent on Γ_{oct}. Nonetheless, an approximate relationship can be derived by combining (10) and (13) and by setting $E_{Rxz} = 0$:

$$\gamma_{oct} \approx 2/3 \sqrt{\cosh(\sqrt{9/2}\,\Gamma_{oct}) - 1}. \quad (14)$$

Figure 4 shows a comparison between this approximate solution (line) and some selected exact results (circles). Errors are <3.5 percent over the range relevant for geologic strains (R_{xy} = 1.0 to 6.0, and S'_y = 0.25 to 4.0). Equation (14) indicates that γ_{oct} has an approximate cylindrical form in strain-magnitude space. Contours of γ_{oct} appear as nested circles in the Nadai diagram (Fig. 2b) and as nested ellipses in the Flinn diagram (Fig. 2a) (see Appendix B for further details).

To conclude, the Nadai diagram provides a better representation of deviatoric strains because distance from the origin is directly related to deviatoric strain magnitude, as represented by E_d, Γ_{oct}, or γ_{oct}. All of these parameters have specific applications where they excel. All are solely a function of the final principal deviatoric strains and are therefore independent of the strain path, principal directions, volume strain, and rotational component of the deformation. The natural deviatoric-strain magnitude E_d provides a correctly-scaled measure of distance in strain-magnitude space. The natural octahedral shear strain Γ_{oct} is conceptually useful because of its relationship to work. The conventional octahedral shear strain γ_{oct} is representative of the average distortion caused by the deformation.

VOLUME-STRAIN SECTIONS

To illustrate the relationship between volume strain and the other strain invariants, we need to examine sections that include the volume-strain axis and thus are orthogonal to the deviatoric section.

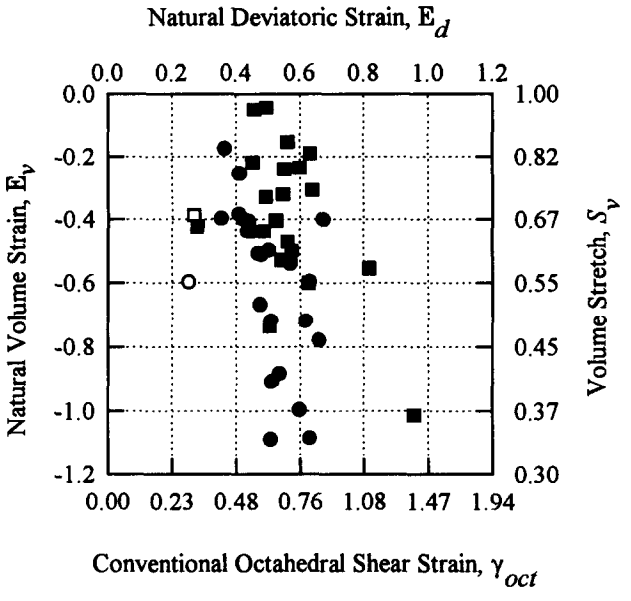

Fig. 5. The E_v-E_d diagram compares volume strain to deviatoric strain. Strain data and plot symbols are explained in Fig. 2. Note that the data show no obvious correlation which suggests that the volumetric and deviatoric strains were decoupled. The primary axes, E_v and E_d, are shown in units of natural strain in order to preserve the correct relative scaling between these two parameters. The secondary axes show the more familiar parameters volume stretch S_v and conventional octahedral shear strain γ_{oct}.

E_v-E_d *diagram*

The first diagram (Fig. 5) compares volume strain with deviatoric strain, using the natural-strain parameters E_v and E_d to ensure that the relative scales of the axes are equivalent and that distance is correctly represented. More familiar measures of volume stretch S_v and conventional octahedral shear strain γ_{oct} are shown on secondary axes (Fig. 5). Note that the E_v-E_d diagram is not a sectional view in the strict sense because the deviatoric-strain component E_d can lie in any direction within the deviatoric section (Fig. 1c). The Franciscan strain data (Fig. 5) show no evidence of a systematic relationship between volume strain and deviatoric strain, which suggests that these two components are controlled by different processes.

S_v-S_y *diagram*

The S_v-S_y diagram (Fig. 6) is useful for distinguishing strain type. Note that distance, as measured by E_t, is distorted in the S_v-S_y diagram because the E_v and E_y axes are not orthogonal in strain-magnitude space (Fig. 1). However, this feature is not needed to distinguish strain type. Therefore, to keep the diagram simple, S_v and S_y are plotted using an orthogonal set of log–log axes with equivalent scaling for both axes.

The diagram (Fig. 6) is divided into four fields. The first two fields, *dilation* ($S_v > 1$) and *compaction* ($S_v < 1$), are defined by volume strain and delimited by the *isochoric strain line* ($S_v = 1$). The second two fields, *constriction* ($S_y < 1$) and *flattening* ($S_y > 1$), are defined by the intermediate principal strain and delimited by the *true plane-strain line* ($S_y = 1$).

The relationship between relative strain and absolute strain can be illustrated by plotting S'_y contours showing the intermediate deviatoric strain (Fig. 6). The equation for each contour is defined by: $E_v = 3(E_y - E'_y)$. As an example, consider a relative strain measurement of $S'_y = 1.2$. The $S'_y = 1.2$ contour shows all possible combinations of S_v and S_y for this deformation. By assuming a volume strain, we can identify the strain type. For instance, if $S_v = 1$, the strain type would be flattening. If $S_v = 0.6$, the strain type would be plane strain.

In my opinion, strain type is best analyzed using the S_v-S_y diagram. Even relative strain data can be portrayed by using the measured S'_y values and assuming some reasonable range for the unmeasured volume strain, such as $S_v = 0.6$ to 1.0. The data can be plotted as line segments parallel to the S'_y contours, or the range of the data can be represented by a bounding box. This approach avoids the problems inherent in using a Flinn or Nadai diagram to interpret strain type (e.g. apparent vs true flattening, etc.).

S_v-S_x *diagram*

The last diagram considered here, the S_v-S_x diagram (Fig. 7), is introduced mainly as a means for examining how volume strain and extension relate to cleavage formation. The diagram is a log–log plot with equivalent scaling used for both axes. Note that the S_v and S_x axes are not orthogonal in strain-magnitude space, so distance is not preserved in the S_v-S_x diagram, except along the S_v and S_x axes.

Cleavage is known to form in an orientation approximately normal to **z**, the maximum contraction direction (e.g. Wood 1974, Ramsay & Huber 1983). With increas-

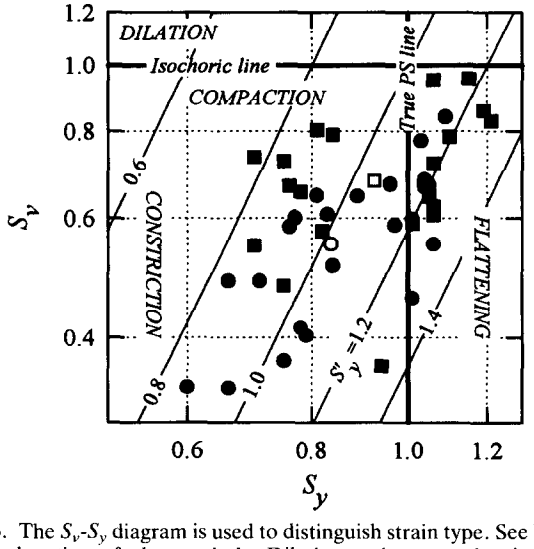

Fig. 6. The S_v-S_y diagram is used to distinguish strain type. See Fig. 2 for explanation of plot symbols. Dilation and compaction indicate volume gain and volume loss, respectively. The intermediate principal stretch S_y is used to distinguish between constriction and flattening. 'True PS line' indicates the true plane-strain line. The diagonal lines show contours of S'_y, the intermediate deviatoric stretch. These contours can be used to represent relative strain data, as explained in the text.

ing deviatoric strain, cleavage fabrics become better developed and more penetrative due, at least in part, to the development of a stronger preferred orientation of the phyllosilicates (Oertel 1983). The maximum axial ratio R_{xz} is used here as a proxy for cleavage intensity because it provides a simple measure of the deviatoric strain in the **xz** section where shear strains are greatest. Consider the following general equation for E_{Rxz}: $E_{Rxz} = 2E_x + E_y - E_v$. If we restrict our discussion to plane-strain deformation ($E_y = 0$), then:

$$E_v = 2E_x - E_{Rxz}. \quad (15)$$

The two terms on the right can be viewed as representing the open and closed parts, respectively, of the deformational system.

To illustrate this problem graphically, contours of R_{xz} are plotted in Fig. 7 as prescribed by (15) for the plane-strain case. The strain paths in Fig. 7 illustrate two end-member cases. Path **A** shows an isochoric plane-strain deformation, whereas path **B** shows a non-extensional plane-strain deformation. The first case is a closed system: the extension in the **x** direction is balanced by shortening in the **z** direction ($E_x = -E_z$, $E_y = E_v = 0$). In the second case, the system is open: the shortening in the **z** direction is entirely balanced by volume loss, resulting in zero extension in the **x** direction ($E_z = E_v$, $E_x = E_y = 0$). As indicated by (15), the closed-system case (**A**) requires half as much strain as the open-system case (**B**) to produce the same R_{xz} ratio. This relationship is illustrated graphically by the relative lengths of arrows **A** and **B** in Fig. 7.

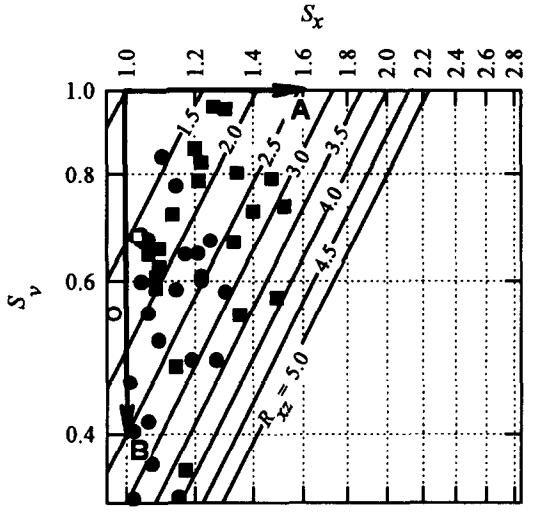

Fig. 7. The S_v-S_x diagram is used to examine the relationship of the maximum axial ratio R_{xz} as a function of volume strain and extension for a plane-strain deformation. R_{xz} provides a simple measure of the distortional strain and thus is used as a proxy for cleavage intensity, which is primarily a function of deviatoric strain magnitude. Two end-member strain paths are shown. Path **A** represents an isochoric deformation where shortening in the **z** direction is balanced by extension in the **x** direction. Path **B** shows an open-system deformation where the shortening in the **z** direction is fully compensated by loss of volume. Distance in the S_v-S_x diagram is distorted except along the S_v and S_x axes. With this in mind, note that the closed-system path (**A**) is half as long as the open-system path (**B**), which indicates the closed-system path only required half the strain magnitude to produce the same distortion (e.g. $R_{xz} = 2.5$). The Franciscan strain data do not follow either of these strain paths. This result is taken as evidence that during cleavage formation, material transport occurred both by local dissolution and precipitation and by wholesale mass loss.

The strain data in Fig. 7 do not fall on either of these strain paths, which indicates that the development of cleavage fabrics, as represented by R_{xz} values, apparently involved both closed- and open-system processes. The dominant mechanism responsible for ductile deformation in these sandstones is pressure solution. Diagnostic fabrics include: (1) the development of discontinuous selvages composed of dark insoluble minerals which form an organized spaced cleavage, (2) truncation of detrital grains along surfaces subparallel to cleavage, and (3) the formation of directed fiber overgrowths in the **x** direction and locally in the **y** direction as well. The open-system behavior is indicated by dissolution and wholesale removal of the more soluble components of the rock, presumably due to regional-scale flow of a solvent fluid phase. The closed-system behavior apparently reflects grain-scale transport of the relatively insoluble components of the rock which are ultimately crystallized as fiber overgrowths. If the solubility of the components that make up the fiber overgrowths is small, then the transport of these components must be restricted to diffusion length scales ($<\sim$10 cm), even if the rates of fluid flow are large.

TENSOR AVERAGE IN STRAIN-MAGNITUDE SPACE

An important limitation of strain-magnitude space is that it does not account for the directional information contained in strain-tensor data. This deficiency is highlighted by comparing a distribution of measured strain data, as represented in strain-magnitude space, with its tensor average. To determine the average strain, we need to account for the strain data as tensors. Paterson & Weiss (1961), Cobbold (1977), and Oertel (1981) have discussed various approaches for estimating such an average. The method used here is outlined in Appendix A.

The tensor averages for the example datasets are indicated by the open symbols in Figs. 2 and 5–7. Note that the averages do not coincide with the modes of their respective sample distributions. As a general rule, the deviatoric strain magnitude indicated by the tensor average will always lie on the low side of the distribution unless the individual strain tensors all have the same orientation. This situation is analogous to vector distributions where the average magnitude of the vectors as determined by a vector-averaging method will always be less than or equal to the scalar average of the vector magnitudes where no account is made for orientation.

This bias does not carry over to the volume-strain data. As an example, consider the tensor averages as shown in Fig. 5, which coincide roughly with the modes of their respective volume-strain distributions. The reason is that volume strain is a scalar measure with no directional properties. Furthermore, the best estimate of the 'average' (i.e. the most likely value) for a real

distribution of volume strain measurements is the logarithmic mean of the volume stretches S_v or the arithmetic mean of the natural volume strains E_v (see Appendix A for details).

The bias of the strain-magnitude distribution in the deviatoric section may have important implications for the plane-strain paradox. Various compilations have shown that relative strain data tend to plot within the oblate field of the Flinn diagram (Ramsay & Wood 1973, fig. 8; Pfiffner & Ramsay 1982, fig. A1). This result appears at odds with the expectation that at the regional scale, geologic deformation should approach, on average, the plane-strain condition. The explanation provided by Ramsay & Wood (1973) is that the compiled data were variably affected by compactional volume strains which would tend to shift the data distribution into the oblate field. An alternative explanation is that this offset is due, at least in part, to the bias introduced by plotting strain distributions on the deviatoric section. One way to account for this bias would be to calculate tensor averages for strain data from individual study areas. This information is not available for the compilations of Ramsay & Wood (1973) and Pfiffner and Ramsay (1982) but probably should be considered in any future compilation.

CONCLUSIONS

This paper has reviewed the use of strain-magnitude space for the analysis of strain data. This approach helps to place the commonly used Flinn and Nadai diagrams into a broader context and provides a more flexible basis for studying the relationship between volume strain and deviatoric strain.

I conclude with the following recommendations:

(1) Total strain magnitude can be decomposed into two orthogonal components, E_v and E_d, which are fundamental scalar measures of the volume strain and average distortion produced by deformation at a material point.

(2) The Nadai diagram is the preferred device for portraying the deviatoric component of strain data because it provides an undistorted representation of the deviatoric section. The use of this diagram should be restricted to the classification of strain symmetry and the examination of deviatoric strain paths.

(3) The S_v-S_y diagram is the preferred tool for discriminating strain type. This diagram is suitable for both absolute and relative strain data. Furthermore, it clearly shows how the interpretation of relative strain data are influenced by assumptions about volume strain.

(4) The E_v-E_d and S_v-S_x diagrams are useful for examining the relationship between deviatoric strain and volume strain as it relates to deformational processes and cleavage formation.

(5) The average of a strain-magnitude distribution should not be equated with the mode of the distribution. Instead, a suitable tensor-averaging method should be used so that direction and magnitude information are fully represented in estimates of average values.

(6) My last recommendation, and perhaps most important, is to encourage a more general use of strain-magnitude space as a basis for constructing strain diagrams and for the interpretation of strain paths. Particular attention should be given to the proper scaling of distance and to the identification of coordinate axes appropriate for the problem at hand.

Acknowledgements—This contribution stems from research at Yale University on pressure-solution deformation in subduction-complex settings. In this context, I thank Jeff Feehan, Bokai Kang and Uwe Ring for discussions and comments on the ideas presented here. The paper benefitted from critical reviews by W. Means and an anonymous reviewer. I am grateful to Uwe Ring for encouraging me to pursue this problem and for allowing me to use our strain data as an example dataset. The research was supported by grants to Brandon from the American Chemical Society (PRF-26621-AC2) and the National Science Foundation (EAR-9005777). My collaboration with Ring was made possible by his fellowship from the Humboldt Foundation.

REFERENCES

Aitchison, J. 1986. *The Statistical Analysis of Compositional Data*. Chapman & Hall, London.

Blake, M. C., Jr., Jayko, A. S., McLaughlin, R. J. & Underwood, M. B. 1988. Metamorphic and tectonic evolution of the Franciscan Complex, northern California. In: *Metamorphism and Crustal Evolution of the Western United States* (edited by Ernst, W. G.). *Rubey Volume*, Prentice-Hall, Englewood Cliffs, New Jersey **8**, 1035–1060.

Brandon, M. T., Cowan, D. S. & Feehan, J. G. 1994. Fault-zone structures and solution-mass-transfer cleavage in Late Cretaceous nappes, San Juan Islands, Washington. In: *Geologic Field Trips in the Pacific Northwest* (edited by Swanson, D. A. & Haugerud, R. A.). *1994 Geol. Soc. Am. Ann. Mtg.* Seattle, Washington, pp. 2L-1–2L-18.

Brimhall, G. H. & Dietrich, W. E. 1987. Constitutive mass balance relations between chemical composition, volume, density, porosity, and strain in metasomatic hydrochemical systems: Results on weathering and pedogenesis. *Geochim. cosmochim. Acta* **51**, 567–587.

Cobbold, P. R. 1977. Description and origin of banded deformation structures. I. Regional strain, local perturbations, and deformation bands. *Can. J. Earth Sci.* **14**, 1721–1731.

Cobbold, P. R. & Percevault, M. 1983. Spatial integration of strains using finite elements. *J. Struct. Geol.* **5**, 299–305.

Elliott, D. 1972. Deformation paths in structural geology. *Bull. geol Soc. Am.* **83**, 2621–2638.

Flinn, D. 1962. On folding during three-dimensional progressive deformation. *Q. Jl. geol. Soc. Lond.* **118**, 385–433.

Flinn, D. 1978. Construction and computation of three-dimensional progressive deformations. *J. geol. Soc. Lond.* **135**, 291–305.

Hobbs, B. E., Means, W. D. & Williams, P. F. 1976. *An Outline of Structural Geology*. John Wiley & Sons, New York.

Hossack, J. R. 1968. Pebble deformation and thrusting in the Bygdin area (Southern Norway). *Tectonophysics* **5**, 315–339.

Hsu, T. C. 1966. The characteristics of coaxial and non-coaxial strain paths. *J. Strain Anal.* **1**, 216–222.

Jaeger, J. C. & Cook, N. G. W. 1979. *Fundamentals of Rock Mechanics*. Third edition, Chapman & Hill, London.

Jayko, A. S. & Blake, M. C., Jr. 1989. Deformation of the Eastern Franciscan Belt, northern California. *J. Struct. Geol.* **11**, 375–390.

Malvern, L. E. 1969. *Introduction to the Mechanics of a Continuous Medium*. Prentice-Hall, Englewood Cliffs.

McKenzie, D. 1979. Finite deformation and fluid flow. *Geophys. J. R. astr. Soc.* **58**, 698–715.

Nadai, A. 1937. Plastic behavior of metals in the strain-hardening range. Part I. *J. appl. Phys.* **7**, 205–213.

Nadai, A. 1950. *Theory of Flow and Fracture of Solids, Volume I*. Second edition, McGraw-Hill, New York.

Nadai, A. 1963. *Theory of Flow and Fracture of Solids, Volume II*. McGraw-Hill, New York.

Oertel, G. 1981. Strain estimation from scattered observations in an inhomogeneously deformed domain of rocks. *Tectonophysics* **77**, 133–150.

Oertel, G. 1983. The relationship of strain and preferred orientation of phyllosilicate grains in rocks—a review. *Tectonophysics* **100**, 413–447.

Paterson, M. S. & Weiss, L. E. 1961. Symmetry concepts in the structural analysis of deformed rocks. *Bull. geol. Soc. Am.* **72**, 841–882.

Pfiffner, O. A. & Ramsay, J. G. 1982. Constraints on geological strain rates: arguments from finite strain states of naturally deformed rocks. *J. geophys. Res.* **87**, 311–321.

Press, W. H., Teukolsky, S. A., Vetterling, W. T. & Flannery, B. P. 1992. *Numerical Recipes in Fortran: The Art of Scientific Computing*. Second Edition, Cambridge University Press, Cambridge, England.

Ramsay, J. G. & Huber, M. I. 1983. *The Techniques of Modern Structural Geology, Volume I: Strain Analysis*. Academic Press, London.

Ramsay, J. G. & Wood, D. S. 1973. The geometric effects of volume change during deformation processes. *Tectonophysics* **16**, 263–277.

Ring, U. & Brandon, M. T. 1994. Ductile strain, mass loss and exhumation of Franciscan rocks. *Geol. Soc. Am. Abst. w. Prog.* **26**, A-73.

Truesdell, C. & Toupin, R. 1960. The classical field theories. In: *Encyclopaedia of Physics* (edited by Flugge, S.). Springer-Verlag, Berlin, **3**, Part 1, 226–793.

Wood, D. S. 1974. Current views on the development of slaty cleavage. *A. Rev. Earth & Plan. Sci.* **2**, 369–401.

APPENDIX A

Tensor average for strain

A method for calculating an average strain tensor is summarized here. The problem can be stated as follows: given a set of strain-tensor measurements randomly sampled from a region that is statistically homogeneous at the scale of sampling (Paterson & Weiss 1961), we seek to estimate the average strain tensor for that region. One definition of the regional average strain is that it corresponds to the tensor that most closely represents the strain experienced by a material line that bounds the sampled region (Cobbold 1977). The only way to calculate this type of average is to reconstruct and integrate the full deformation, strain plus rotation, within the region using the strain-compatibility relationships (e.g. Cobbold & Percevault 1983). This approach requires: (1) identification of domains within the sampled region where strain is relatively homogeneous, and (2) accurate determination of the average strain within each domain. In most cases, strain data are not dense enough nor the deformation sufficiently homogeneous at the domain scale to warrant such an approach. Thus, these considerations have led me to explore a simpler approach where the rotational component of the deformation is ignored. Numerical experiments are used to determine the biases introduced by this simplification. Oertel (1981) presented a useful discussion of the problems associated with calculating average strain; the method proposed here is similar to his 'directed method'.

A general finite deformation is usually described by $\mathbf{F} = \mathbf{VR}$, where $\mathbf{F}$ is the deformation-gradient tensor, $\mathbf{V}$ is the left-stretch tensor, and $\mathbf{R}$ is the rotation tensor (Malvern 1969, p. 173). A simple modification provides an explicit account for relative strain data: $\mathbf{F} = (\mathbf{V}'S_v^{1/3})\,\mathbf{R}$, where $\mathbf{V}'$ is the left deviatoric stretch tensor and S_v is the volume stretch. The objective is to estimate tensor averages for $\mathbf{V}$ or $\mathbf{V}'$ using only absolute or relative strain data, as the case may be. The reliability of the estimated tensor average depends heavily on the assumption that the distribution of sampled strain tensors is representative of the parent population. For instance, if some component of the deformation field is not represented by the measured strain data—such as brittle deformation caused by widely spaced faults or ductile deformation in poorly sampled lithologies with unusual rheological properties—then the tensor average will be biased. This represents a sampling problem and not a deficiency of the averaging method itself.

To calculate the strain-tensor average, we first need to transform each of the individual tensor measurements into a natural-strain tensor $\mathbf{H}$ (Truesdell & Toupin 1960, p. 269), which Elliott (1972) called the Hencky strain matrix. The principal values for $\mathbf{H}$ are the natural principal strains E_x, E_y, E_z, and the principal directions are the same as those for $\mathbf{V}$. To state this relationship explicitly, consider the principal form of $\mathbf{V} = \mathbf{T}\,\Lambda_V\,\mathbf{T}^t$, where $\Lambda_V = \mathrm{DIAG}\{S_x, S_y, S_z\}$ and $\mathbf{T}$ is a 3×3 transformation matrix whose columns are unit vectors representing the three principal strain directions. DIAG{} defines the components of a diagonalized square matrix, and $\mathbf{T}^t$ is the transpose of $\mathbf{T}$. The Hencky strain tensor is then defined as: $\mathbf{H} = \mathbf{T}\,\Lambda_H\,\mathbf{T}^t$, where $\Lambda_H = \mathrm{DIAG}\{E_x, E_y, E_z\}$.

The tensor average is determined by a simple component-by-component average of $\mathbf{H}$: $\mathrm{AVE}\langle\mathbf{H}\rangle = (1/n)\,\Sigma\mathbf{H}_i$, where $\mathbf{H}_i$ represents the ith strain tensor in a distribution containing n tensor samples. Eigenvector decomposition of $\mathrm{AVE}\langle\mathbf{H}\rangle$ gives the directions and magnitudes of the average natural principal strains. This procedure can also be used to estimate the tensor average for $\mathbf{V}'$ by introducing a deviatoric version of the Hencky tensor, $\mathbf{H}'$ with principal values E'_x, E'_y, E'_z.

I have tested this averaging method using synthetic data generated by introducing stochastic variations into a general three-dimensional rotational deformation. The deformation is specified by a velocity-gradient tensor $\mathbf{L}$ that remains constant at a material point but otherwise varies from point-to-point. The finite deformation $\mathbf{F}$ at the material point is determined by numerically integrating the material derivative $\mathrm{D}\mathbf{F}/\mathrm{D}t = \mathbf{LF}$ (McKenzie 1979). The simulation can be viewed as representative of a deforming material where each material point sees a steady deformation but the deformation of the material body as a whole is inhomogeneous. Note that the simulation can ignore the issue of strain compatibility because strain and rotation are fully specified at each sampled point and because we can invoke arbitrary deformation gradients for the regions that lie between the sampled points. This approach is fairly simple minded, but it provides a reasonable first-order representation of the variations that might exist in a real strain-tensor distribution.

The first step in generating a synthetic dataset is to produce a distribution of $\mathbf{L}_i$ samples where $i = 1$ to n. The components of the expected velocity gradient tensor $\langle\mathbf{L}\rangle$ are independently perturbed using Gaussian variants to generate each $\mathbf{L}_i$ sample. Integration of the $\mathbf{L}_i$ samples gives a distribution of $\mathbf{F}_i$ samples. The expected deformation-gradient tensor $\langle\mathbf{F}\rangle$ is defined by the integration of $\langle\mathbf{L}\rangle$. $\langle\mathbf{F}\rangle$ is then decomposed to find the expected left stretch tensor $\langle\mathbf{V}\rangle$.

Let us examine some results. Consider a case where the average deformation, as indicated by $\langle\mathbf{L}\rangle$, is coaxial but the $\mathbf{L}_i$ distribution includes both coaxial and noncoaxial samples. This case is analogous to a deformation that is coaxial at the regional scale, but is characterized by folding (i.e. variable noncoaxial deformation) at the local scale. The numerical simulations show that the tensor-averaging method produces unbiased estimates of $\langle\mathbf{H}\rangle$ and $\langle\mathbf{H}'\rangle$, and their counterparts $\langle\mathbf{V}\rangle$ and $\langle\mathbf{V}'\rangle$.

Now consider a case where the average deformation, as prescribed by $\langle\mathbf{L}\rangle$, is noncoaxial. In this case, the tensor-average method shows significant biases, but this result is not unexpected given that the averaging scheme lacks information about the rotational component of the deformation. My experience to date indicates that for strain magnitudes and internal rotations typical of geologic deformation, the orientation of the average principal directions are accurately estimated, but the average principal stretches are biased, but usually by no more than 10–20% of their magnitudes. For example, consider an isochoric simple-shear deformation that results in an average deformation with principal stretches of 3.33, 1.0 and 0.30 and an internal rotation of 57°. For a representative simulated distribution with $n = 10{,}000$, the tensor-average method gives principal stretches of 3.0, 1.03 and 0.36. The biases are systematic in that the estimates for S_x are always on the low side, and those for S_z are always on the high side.

As for volume strain, the tensor-average method produces an estimate that is identical to the average of the natural volume strains, $\mathrm{AVE}\langle E_v\rangle = (1/n)\Sigma(E_v)_i$. This result is entirely expected given that volume stretch S_v is a ratio quantity. Aitchison (1986) showed that the expected value for a distribution of ratio measurements is usually best estimated by the logarithmic mean, which in our case would be: $\mathrm{AVE}\langle\ln S_v\rangle = (1/n)\,\Sigma\ln(S_v)_i$.

APPENDIX B

Constructing the Nadai diagram

Hsu (1966) and Hossack (1968) proposed a radial version of the Nadai diagram using E_d and the Lode's parameter, ν. Unfortunately, radial plots are not supported in most graphics programs. The version of the Nadai diagram used here (Fig. 2b) is based on an orthogonal log–log plot, an option available in almost all graphics programs.

Another advantage is that it uses familiar coordinate variables, R_{xz} and S'_y, which help convey more information. The details for constructing this version of the Nadai diagram are outlined here.

Start with a square plot and logarithmic axes. We need to adjust the ranges for R_{xz} and S'_y to ensure that the two axes have equal lengths in E_d units. R_{xz} is set to range from 1 to MAX(R_{xz}), which is the maximum observed value for the data. The minimum and maximum values for S'_y are determined by:

$$\text{MAX}(E'_y) = \sqrt{1/12}\,\text{MAX}(E_{Rxz}), \quad \text{and} \quad \text{MIN}(E'_y) = -\sqrt{1/12}\,\text{MAX}(E_{Rxz}). \tag{B1}$$

These equations account for the scaling relationships implicit in (9) and the fact that the S'_y axis is centered on one. The borders of the accessible sector of the deviatoric section are defined by:

$$E_{Rxz} = -3\,E'_y \quad \text{and} \quad E_{Rxz} = 3\,E'_y, \tag{B2}$$

which represent the E'_x and E'_z axes, respectively (Fig. 1c). If the plot is correctly scaled, these lines will lie at 30° on either side of the vertical.

To add contours of conventional octahedral shear strain (Fig. 2b), we need to specify E_d as a function of γ_{oct}. The approximate relation (14) can be reorganized by using identities and inverse relationships for the hyperbolic functions and by substituting $E_d = \sqrt{3/4}\,\Gamma_{oct}$ to give:

$$E_d \approx \sqrt{1/6}\ln(\eta + \sqrt{\eta^2 - 1}), \tag{B3}$$

where $\eta = (9/4)\gamma_{oct}^2 + 1$. To plot a specific γ_{oct} contour, first determine the radius of the contour in terms of E_d using (B3). Next, convert to coordinates of E_{Rxz} and E'_y using:

$$E_{Rxz} = \sqrt{2}\,E_d\cos\beta, \quad \text{and} \quad E'_y = \sqrt{2/3}\,E_d\sin\beta, \tag{B4}$$

To draw the contour, calculate values of E_{Rxz} and E'_y as β varies from −30° to +30° (Fig. 1c).